World Academy of Science, Engineering and Technology
International Journal of Mechanical and Mechatronics Engineering
Vol:11, No:8, 2017

Numerical Investigation of Dynamic Stall over a Wind Turbine Pitching Airfoil by Using OpenFOAM

Mahbod Seyednia, Shidvash Vakilipour, Mehran Masdari

Abstract**—**Computations for two-dimensional flow past a stationary and harmonically pitching wind turbine airfoil at a moderate value of Reynolds number (400000) are carried out by progressively increasing the angle of attack for stationary airfoil and at fixed pitching frequencies for rotary one. The incompressible Navier-Stokes equations in conjunction with Unsteady Reynolds Average Navier-Stokes (URANS) equations for turbulence modeling are solved by OpenFOAM package to investigate the aerodynamic phenomena occurred at stationary and pitching conditions on a NACA 6-series wind turbine airfoil. The aim of this study is to enhance the accuracy of numerical simulation in predicting the aerodynamic behavior of an oscillating airfoil in OpenFOAM. Hence, for turbulence modelling, *k-ω-SST* with low-Reynolds correction is employed to capture the unsteady phenomena occurred in stationary and oscillating motion of the airfoil. Using aerodynamic and pressure coefficients along with flow patterns, the unsteady aerodynamics at pre-, near-, and post-static stall regions are analyzed in harmonically pitching airfoil, and the results are validated with the corresponding experimental data possessed by the authors. The results indicate that implementing the mentioned turbulence model leads to accurate prediction of the angle of static stall for stationary airfoil and flow separation, dynamic stall phenomenon, and reattachment of the flow on the surface of airfoil for pitching one. Due to the geometry of the studied 6-series airfoil, the vortex on the upper surface of the airfoil during upstrokes is formed at the trailing edge. Therefore, the pattern flow obtained by our numerical simulations represents the formation and change of the trailing-edge vortex at near- and post-stall regions where this process determines the dynamic stall phenomenon.

Keywords**—**CFD, Moderate Reynolds number, OpenFOAM, pitching oscillation, unsteady aerodynamics, wind turbine.

I. Introduction

TECHNICALLY, the components of wind turbines are exposed to frequently dynamic loadings during their operation periods. The loads are due to the shear stress of the wind, turbulent flow, upwind vortices, and gusts, which lead to some unsteady phenomena like dynamic stall. The unsteady aerodynamic effects are the primary source of the fatigue and failure in a wind turbine component such as the blades [1], [2]. Obtaining optimal wind turbine blades design regarding the flow condition and aerodynamic parameters will lead to lower costs and maximizes the extracting energy from the system. Therefore, Computational Fluid Dynamics (CFD) along with experimental tests is utilized to improve the design and performance of wind turbines. CFD has become one of the most important techniques in aerodynamics, and it is widely used to simulate and analyze the aerodynamic phenomena. In recent years, CFD has been utilized by many researchers in wind energy industry as well as in the aerospace.

When a wind turbine blade is subjected to an unsteady motion such as pitching or plunging, a series of separations and reattachments can occur which lead to dynamic stall occurrence. Under the dynamic stall effects, the stall angle of an airfoil is found to be higher than the normal static stall angle. In unsteady conditions, the lift force can still be maintained even at Angles of Attack (AoA) higher than static stall angle. The so-called dynamic stall is of great importance in unsteady aerodynamics of aircraft, helicopter, wind turbine and turbomachinery.

In the 1970s and the early 1980s, McAlister et al. [3] and McCroskey [4] et al. conducted a series of experimental analysis of dynamic stall phenomenon in pitching airfoils. In the 1980s, McCroskey carried out a thorough physical analysis of dynamic stall in two review papers [5], [6]. The flow analysis around a pitching airfoil revealed the formation of a Leading-Edge Vortex (LEV) where the growth of this vortex lets the lift and drag coefficients rise beyond the static stall angle. Then, the travelling and shedding of the LEV from the suction side of the airfoil causes dramatically drop of the lift coefficients, namely dynamic stall occurrence. The reattachment of the flow to the suction surface occurs after the full stall. Since then, both the experimental and numerical analyses of unsteady flow properties and unsteady phenomena occurring in pitching airfoils have been conducted extensively by many researchers and it continues to be the focus of study today.

Most of the previous researches on dynamic stall and pitching airfoils have been devoted to high Reynolds number flow $(\mathrm{Re} \geq 10^6)$ or the flows with Mach number greater than 0.3 where the compressibility effects have impact on the flow structures [7]-[11]. Also, some researches carried out on low-Reynolds numbers concerning the laminar flows where the flow structures are far away from the turbulent or high-Reynolds flow [12], [13]. Although the modern Horizontal Axis Wind Turbines (HAWT) may operate in the range of high-Reynolds number, the small-medium turbines work in the range of moderate-Reynolds number (10^5) generally. The flow structure in this regime is highly nonlinear [14], and the dynamic stall occurs according to the vortex formation on the upper surface and the transition of laminar flow to turbulent in boundary layer. There have been very few studies in the literature, either numerically or experimentally, concerning the

Mahbod Seyednia and Mehran Masdari are with the Department of Aerospace Engineering, Faculty of New Sciences and Technologies, University of Tehran, Tehran, Iran (e-mail: m.seyednia@ut.ac.ir, m.masdari@ut.ac.ir).

Shidvash Vakilipour is with the Department of Aerospace Engineering, Faculty of New Sciences and Technologies, University of Tehran, Tehran, Iran (phone: 989121326951, e-mail: vakilipour@ut.ac.ir).

pitching airfoils in moderate-Reynolds number regime [15]-[20].

The studies on pitching airfoil and dynamic stall express that the generality of what is happening is the same for all airfoils. However, based on the flow regime and airfoil type, the place of vortex formation, the way how it changes and moves, and the transition point in boundary layer can be different, and hence, the study of different airfoils in different flow regimes must be thoroughly investigated. With a focus on aerodynamics of wind turbines, most of the airfoils studied in the literature are NACA0012 [7], [9], [10], [15]-[20], NACA0015 [8]-[10] and the NREL S809 [11], [21], [22] airfoils which are very common in the wind turbine industries. Beside these airfoils, NACA 6-series airfoils are widely utilized in wind turbines, while very few studies are conducted over unsteady aerodynamics of these airfoils.

Most of the numerical researches on pitching airfoils in turbulent regimes have implemented the URANS equations together with the turbulence models. Due to high computational costs, few researches can be found in literature which have implemented Large-Eddy Simulation (LES) [23], [24]. Moreover, to the best of the authors' knowledge, very few studies have been conducted on a NACA 6-series airfoil pitching at moderate Reynolds number using OpenFOAM package. This open-source package provides the facility to solve either incompressible or compressible flows by finite volume method. Different turbulence models and boundary conditions can be added to the package [25].

The objective of this study is to simulate the unsteady phenomena of a sinusoidal pitching NACA 6-series airfoil in OpenFOAM package. But firstly, the experimental and numerical results of a pitching NACA 0012 airfoil at moderate Reynolds number published in [15], [17] are used to confirm the correct simulation of an oscillating airfoil in OpenFOAM package. Afterward, the numerical simulation of a NACA 6-series airfoil will carry out. The aerodynamic and pressure coefficients are compared quantitatively with the experimental data. The mentioned airfoil is brought out of the critical section of a horizontal wind turbine blade.

II. Numerical Simulation

A. Simulation Cases and Key Parameters

In this study, a static and an oscillating NACA 6-series airfoils are simulated to investigate the unsteady aerodynamic behavior occurring in both stationary and pitching conditions. For stationary case, the lift, drag and pressure coefficients around the airfoil are calculated and plotted. Then, the sinusoidal oscillation of the airfoil is simulated. The harmonic motion of the airfoil is described by:

$$\alpha(t) = \alpha_0 + d\sin(\omega t) \tag{1}$$

where α_0 and d are the mean angle of attack and the amplitude in degree and ω is the angular frequency of the oscillation in rad.s^{-1}. The rotation axis is the quarter-chord.

For unsteady aerodynamic cases, a dimensionless number known as reduced frequency is defined to represent the unsteadiness of the problem. The reduced frequency is given by:

$$k = \frac{\omega.c}{2v} \tag{2}$$

where c is the chord length in meter, and v is the freestream velocity in m.s^{-1}.

The quasi-steady characteristics of the airfoil undergoing pitching motion with the reduced frequency of 0.025 are investigated in pre-, near- and post-static stall regions. The details of the simulated cases are given in Table I.

TABLE I
Test Cases Studied on Sinusoidal Pitching Airfoil

Case	Mean Angle of Attack (deg)	Amplitude (deg)
Pre-static stall	5	2
Near-static stall	5	8
Post-static stall	10	8

For all the cases of NACA 6-series airfoil, the freestream velocity is 30 m/s. The Reynolds number is 400000. The hysteresis loops of the lift and drag coefficients are plotted for all the cases. The pressure coefficient distributions around the airfoil are plotted at different AoAs. The streamlines are investigated for the near- and post-stall cases. The comparison of the numerical results and the corresponding experimental data are carried out for all the cases. It is worth mentioning that due the experimental measurements, the drag coefficients include only the pressure term. Also, the error and uncertainty analyses of the experiments have been conducted for more accurate study of the pressure distribution around the airfoil. The maximum error in experimental data is 5% which is considered for all the experimental data. The error is due to the calibration, measurement, and pressure sensor errors.

B. Numerical Solver

Although Direct Numerical Simulation (DNS) is the most advanced and accurate method in turbulence simulations, the demand of huge computing systems prevents the fluid dynamics scientists from implementing this method in large simulations, the dynamic motion of objects in particular. LES is less costly than DNS, but still very computationally expensive for complex unsteady simulations. As a result, the URANS method seems to be the most suitable approach to simulate an oscillating airfoil with an acceptable computational cost [11], [26], [27]. Hence, the URANS method along with the turbulence models is employed in the current study.

In this study, using OpenFOAM package, the governing equations are considered in the form of 2D incompressible unsteady Navier-Stokes equations discretized based on finite volume method. The temporal term is discretized by the second-order implicit scheme. The PIMPLE algorithm, the combination of the SIMPLE and PISO algorithms, is implemented for pressure-velocity coupling. Based on the iterations in each time step, the PIMPLE algorithm lets the

simulation work with higher Courant number and consequently, larger time step size can be chosen to speed up the simulation [25]. However, due to the unsteady nature of oscillating airfoils, time step independence study has been carried out to ensure the unsteady phenomena occurred in our simulations are captured. Time step sizes of 10^{-3}, 10^{-4}, and 10^{-5} were investigated and the results indicated (Fig. 1) that no changes happened from 10^{-4} to 10^{-5}. So, the larger time step size was considered for all the simulations in this study.

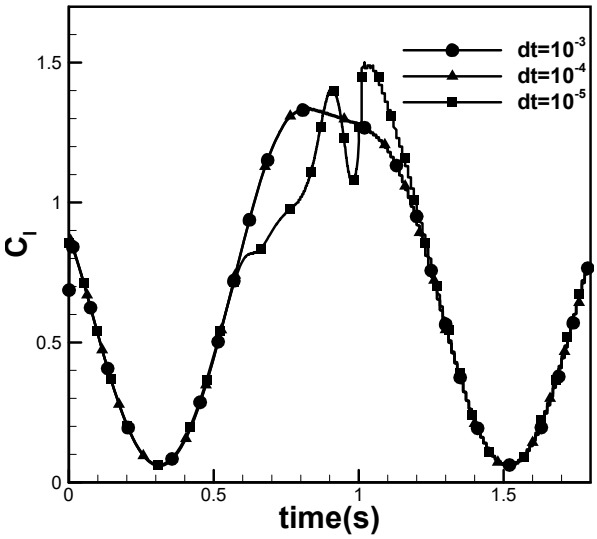

Fig. 1 Time-independence of the pitching airfoil at near-static stall region

One-equation Spalart-Allmaras [28] and two-equation shear stress $k-\omega$ models named $k-\omega-SST$ [29] are two appropriate turbulent models to simulate the external flows, the flow around airfoils in particular. To the best of our knowledge and based on other numerical studies [16], the drawback of Spalart-Allmaras model compared to $k-\omega-SST$ model emerges in simulating the separation phenomenon and vortex formation, and consequently, less-accurate estimation of aerodynamic coefficients takes place. Therefore, in the current study, the two-equation $k-\omega-SST$ model is applied to close the system of URANS equations. This turbulence model is a well-known and approved model in simulation of the unsteady phenomena and capturing the flow structures occurring in oscillating airfoils [13], [16], [17], [20], [30]. Although the standard $k-\omega-SST$ model is a fully-turbulent model, in this study, a low-Reynolds correction is applied to accommodate the transitional process. Using this correction, the turbulent viscosity is damped by the coefficient α^*. The turbulent viscosity is calculated as below [17]:

$$\mu_t = \frac{\rho k}{\omega}\frac{1}{\max[1/\alpha^*, SF_2/\alpha_1\omega]} \tag{3}$$

where

$$\alpha^* = \frac{0.024+(\mathrm{Re}_t/6)}{1+(\mathrm{Re}_t/6)} \tag{4}$$

and

$$\mathrm{Re}_t = \frac{\rho k}{\mu\omega} \tag{5}$$

It is worth mentioning that the $k-\omega-SST$ model with low-Re correction is not available in OpenFOAM versions. So, this model has been added to OpenFOAM by the authors of this study.

C. Geometry and Computational Grid

The geometry of the airfoil is extracted from the critical section of a 660-kW horizontal wind turbine blade installed for electricity generation. Fig. 1 shows the geometry of the airfoil. The chord length of the airfoil is 0.25 m.

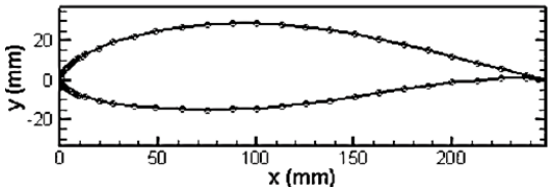

Fig. 2 Airfoil geometry

The computational domain was simulated as a 2D "O-Mesh" topology with the diameter of 25 times that of the chord length. All the meshes in this study were generated by GAMBIT software. Four computational grids with different number of cells and nodes around the airfoil were generated for grid independence analysis. The grid independence is studied by generating two different O-type meshes with unstructured cells and one typical C-type grid with structured cells. In all the meshes, structured grid has been implemented for boundary layer analysis. Delaunay triangulation method was implemented to generate the unstructured cells. The height of the first cell adjacent to the airfoil has been considered in a way that the y^+ values are less than 1 all around the body.

TABLE II
DETAILS OF GENERATED GIRDS WITH LIFT COEFFICIENT VALUES IN STATIC CASE

Grid Number	Grid Size	Number of Nodes around Airfoil	Cell Type	c_l (α=8°)	c_l (α=14°)
G1	70000	700	Unstructured	1.1388	1.3129
G2	110000	1000	Unstructured	1.1393	1.3188
G3	153000	500	Structured	1.1367	1.3123

A grid study was done to check the sensitivity of the stationary and pitching simulations to the grid size. For stationary case, the aerodynamic coefficients were calculated for all the grids at static AoA of 8° (with no separation) and 14° (with significant separation). For oscillating airfoil, the aerodynamic coefficients of four grids in a near-static stall

case (α_0=5°, d=8°) were compared to confirm the grid independence of the results. The details of the generated grids with the values of the static lift coefficients can be found in Table II. Fig. 3 depicts the grid independence of the pitching airfoil in one cycle. The grid independence analysis suggests G1 as the appropriate grid for this study. Fig. 4 depicts the final grid with 70000 cells.

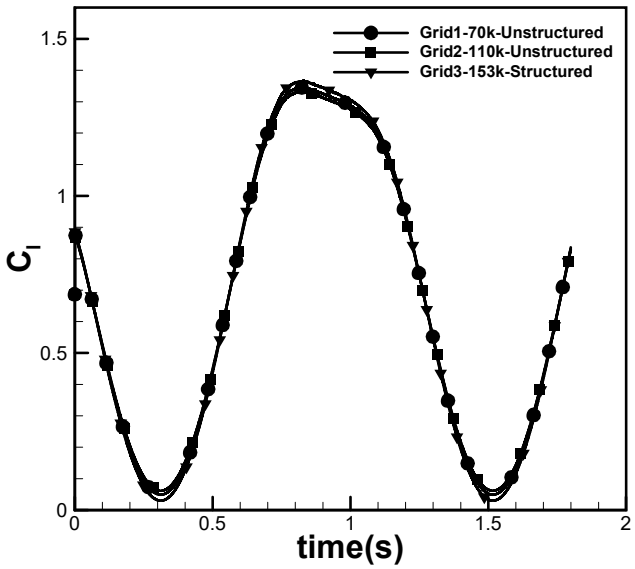

Fig. 3 Grid-independence of the pitching airfoil at near-static stall region

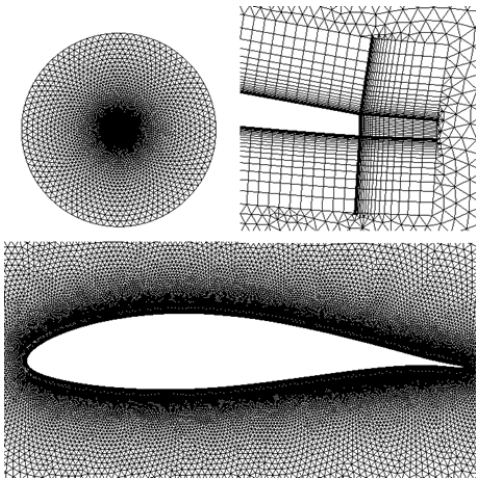

Fig. 4 70k-cell Mesh topology

For oscillating airfoil, the pitching motion of the airfoil is pre-defined, and then, using dynamic mesh technique, the grid nodes and cells near the airfoil are moved to accommodate the deformation of the domain due to the airfoil motion. To this end, the PIMPLEDyMFoam solver is implemented in this study to simulate the motion of the airfoil. The integral form of the conservation equation of property Ø over an arbitrary moving control volume is

$$\frac{d}{dt}\int_{V_C}\phi dV_C + \int_A dA.(u-u_b)\phi = \int_{V_C}\nabla.(\Gamma\nabla\phi)dV_V \quad (6)$$

where u is the velocity vector of the fluid, A is the outward pointing surface area vector, u_b is the boundary velocity vector of the cell face and Γ is the diffusivity coefficient. The local boundary velocity (u_b) is obtained by the interpolation of the velocity points (u_p) which are the vertices of the control volume. The Laplacian operator is applied to determine the motion of the vertices of a control volume. Equation (7) governs the motion of a vertex with the diffusivity γ.

$$\nabla.(\gamma\nabla u_p) = 0 \quad (7)$$

The boundary condition for this equation is defined by the pre-defined motion of the airfoil. As a result, the final position of a vertex is calculated using u_p as shown in (8)

$$x^{n+1} = x^n + u_p\Delta t \quad (8)$$

The diffusivity γ has great impact on the quality of mesh deformation. So, to enhance the mesh deformation quality, the diffusivity is determined as a function of the mesh quality value [31].

D.Numerical Simulation Validation

To ensure the correct implementation of OpenFOAM for simulating a pitching airfoil, a NACA 0012, the well-documented airfoil in pitching oscillation is utilized. The Reynolds number for this case is 135000, same with the numerical results of [17] and experimental data of [15]. The airfoil with the chord length of 15 cm has a pitching motion around 10° mean AoA with the amplitude of 15°. The freestream velocity is 14 m/s, and the reduced frequency of the oscillation is 0.1.

Fig. 5 shows that, during the upstroke motion of the airfoil, the lift and drag coefficients of the current simulation match more accurately with the experimental data compared to the results of [15]. Using $k-\omega-SST$ model with low-Re correction, the slopes of the lift and drag coefficient diagrams have the same values of the experimental data. The maximum lift and the onset of fully separation of the dynamic stall vortex from the upper surface of the airfoil occur at α=22°. After the separation and travelling the vortex toward the trailing edge region, the lift coefficient drops abruptly. As seen in Fig. 5-(a), the lift stall of the numerical simulations occurs earlier than experimental stall, like other numerical reports [17]-[20]. This is due to the drawback of the URANS method in simulating the eddies and vortex formation. The turbulence models cannot accurately predict the transitional process of the flow from laminar to turbulent. Also, the process of vortex formation, separation and shedding of that vortex cannot be modelled thoroughly by turbulence models. The real shape of the trailing edge can be another reason of the discrepancy.

As seen in Fig. 5 (a), after the sudden drop-off in lift coefficient, a secondary vortex forms at the end of the upstroke motion where this vortex leads to a relative increase in lift coefficient. At the start of the downstroke motion, the secondary vortex separates then, the lift coefficient drops

gradually by decreasing of the AoA. The red circle on Fig. 5 (a) represents the crossover of upstroke and downstroke motions where the separation of dynamic stall vortex and the secondary vortex coincide. This region has a good agreement with the numerical results of [17].

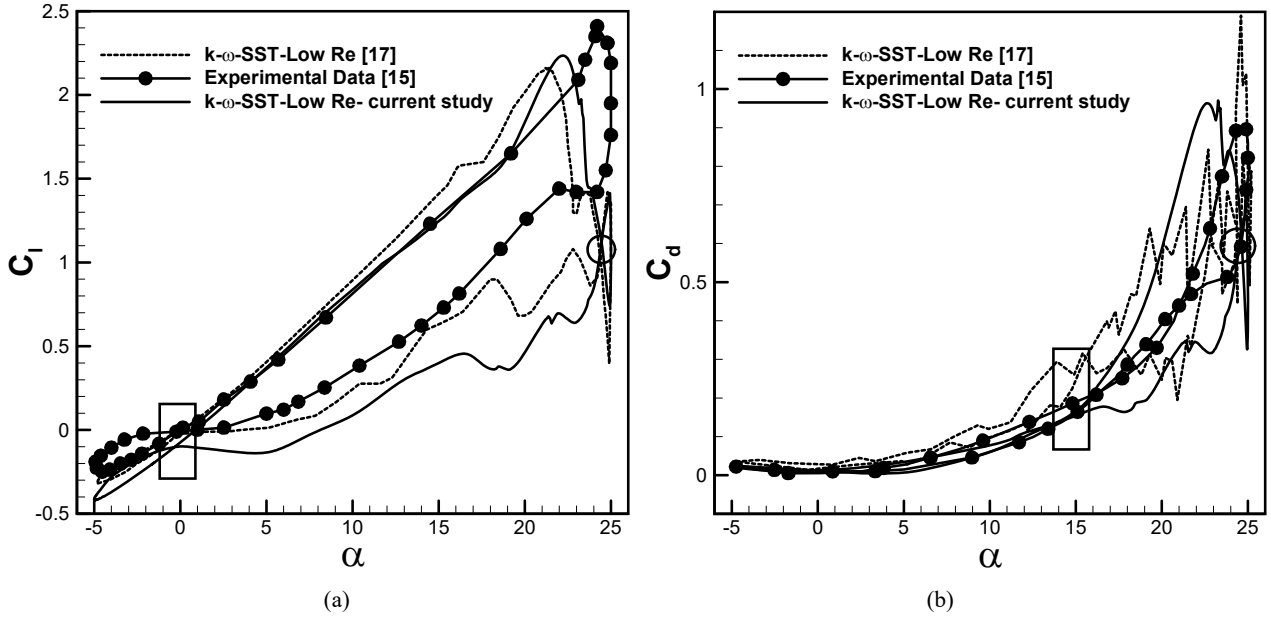

(a) (b)

Fig. 5 Comparison of aerodynamic coefficients of current numerical simulation and corresponding results of [15], [17]

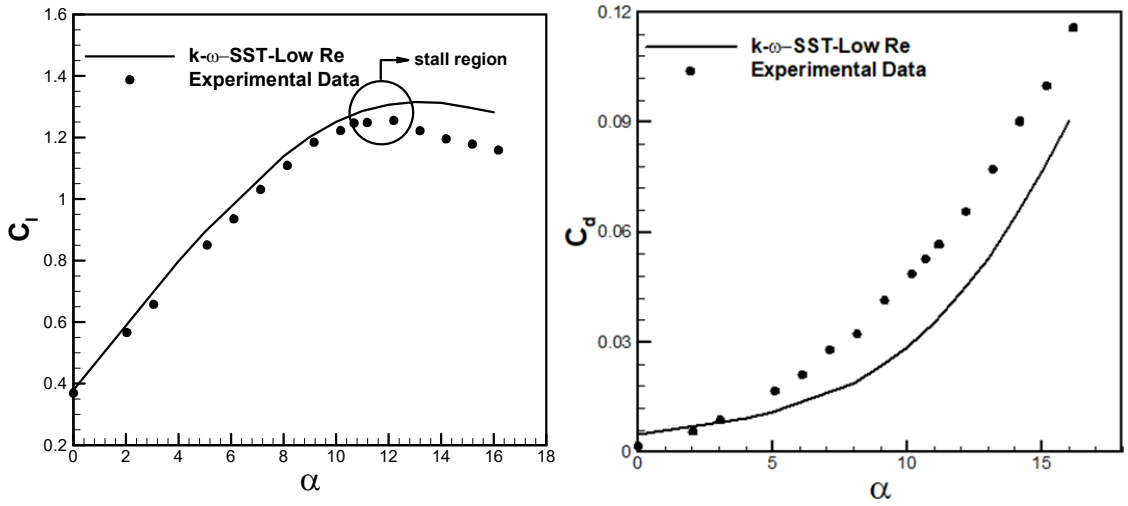

(a) (b)

Fig. 6 Comparison of aerodynamic coefficients of numerical results by $k-\omega-SST$ with low-Re correction turbulence models and experimental data

The intersection point at α≈0°, represented by the red rectangle, shows the turning of the phase lead of lift into the lag one. At this region, the reattachment of flow occurs again at the end of the downstroke motion. The numerical results predict the angle of reattachment correctly as the experimental data and the result of [17]. It is worth mentioning that, according to our studies, this reattachment region with increase of lift coefficient cannot be observed by the standard $k-\omega-SST$. The implementation of the low-Re correction leads to higher dissipation in turbulent viscosity and consequently, the laminar flow starts to exist on the surface of the airfoil, and the lift coefficient increases slightly.

The drag coefficient diagram (Fig. 5 (b)) shows that the result of [17] has some unphysical fluctuations in drag values, while the present study predicts the drag values more accurately. The crossovers of upstroke and downstroke motions, represented by red circle and rectangle, have a good agreement with the numerical results of [17]. However, better prediction of drag coefficients is carried out in the current numerical simulation; more particularly for α≤17° and also the

estimation of the maximum drag coefficient.

III. Results

A. Static Airfoil

In this part, the aerodynamic coefficients of the stationary wind turbine airfoil and the stall point are compared with the corresponding experimental data. Fig. 6 depicts the lift and drag coefficients versus the AoA from 0° to 16°.

For α≤11°, the angles before stall occurrence, the numerical predictions of the lift coefficient are reasonably close to the experimental data, likely where little or no vortex separation is present. After stall point, however, the numerical results start to deviate from the experimental curve. Almost all RANS turbulence models overpredict the lift coefficient after stall point. This discrepancy can likely be attributed to the drawback of RANS and URANS models which cannot capture the vortices formed on the airfoil at high AoAs, and hence, the values of aerodynamic coefficients are partially inconsistent with the experimental data. However, it is observable from Fig. 6 (a) that the values of aerodynamic coefficient from the numerical simulation are qualitatively in very good agreement with the experimental data.

According to Fig. 6 (b), the pressure drag coefficients are slightly higher than the corresponding experimental data for α≤4°. Assuming fully turbulent flow in turbulence models leads to this overprediction. However, for higher AoAs where eddies and vortices start to grow, the numerical results underestimate the pressure drag values. Mesh refinement at boundary layer, decreasing the y^+ values to less than 1 and also choosing correct turbulence parameters are implemented to remove these discrepancies. Nevertheless, some deviations are observed in aerodynamic coefficient curves. In addition to the incapability of the RANS turbulence models in prediction of flow behavior near and post stall, the error due to the experimental equipment and wall effects may cause the deviations. The differences observed in lift prediction such as higher stall angle and the overprediction of the lift beyond stall and also, the underprediction of the drag coefficients have been noticed in other numerical studies [11], [32].

B. Pitching Airfoil; Pre-Static Stall Case

As seen in the previous section, the angle of static stall is beyond 10°. So, to study the pre-static stall region, the airfoil is located at α=5° pitching with the amplitude of 2°. Based on the value of the reduced frequency (0.025), the aerodynamic coefficients are phase-lag, and hence, the hysteresis loop of the lift coefficient must be counterclockwise. Fig. 7 suggests the comparison of the numerical predictions of the lift and pressure drag coefficients with the corresponding experimental values.

It is noticeable that the numerical predictions of the lift coefficient are slightly greater than the experimental values. The slope of the lift coefficient loop, however, agrees well with the slope of the experiment. The differences between the lift values were also observed in the static case. The lift coefficient curve of the static airfoil is plotted in Fig. 7 (a) as well to evaluate the performance of the $k-\omega-SST$ with low-Re correction in both stationary and oscillating airfoils. As seen, the static curves of the lift and drag coefficients pass through the corresponding numerical results. Fig. 7 (b) suggests that the drag coefficients have good agreement with the corresponding experimental value at low AoA, but the differences increase at higher AoAs. The reasons of the discrepancy were discussed in the previous section.

The pressure distributions of the airfoil for two AoAs in the upstroke and downstroke motions are shown in Fig. 8 to validate the numerical results and provide a better insight as to the flow. The comparison indicates that the numerical predictions agree well with experimental values on most of the points in the lower surface. However, some slight deviations can be observed on the upper side which can be attributed to the roughness of the real model and also the restrictions of installing the pressure sensors on the airfoil in some regions.

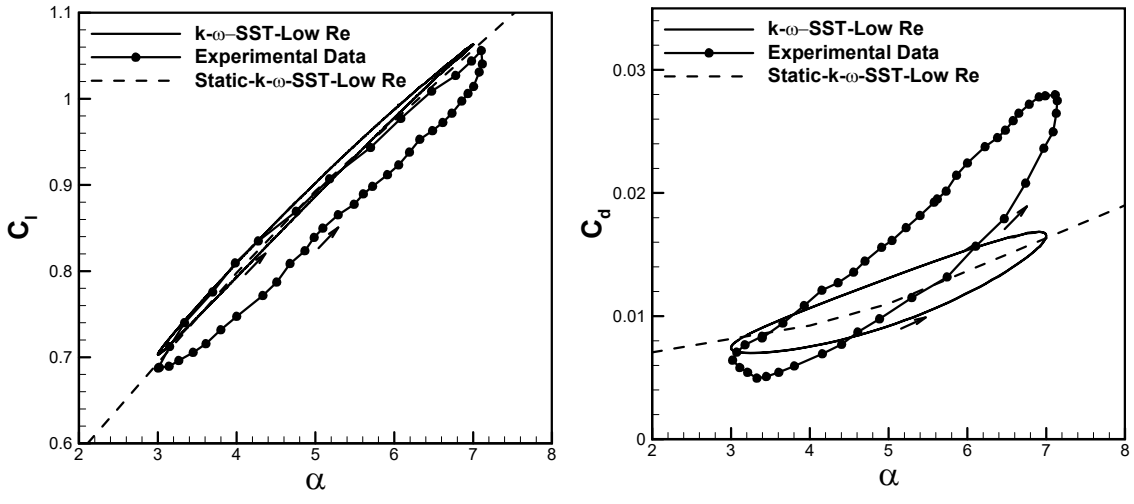

(a) (b)

Fig. 7 Aerodynamic coefficients-1st test case- α_0=5°, d=2°, k=0.025

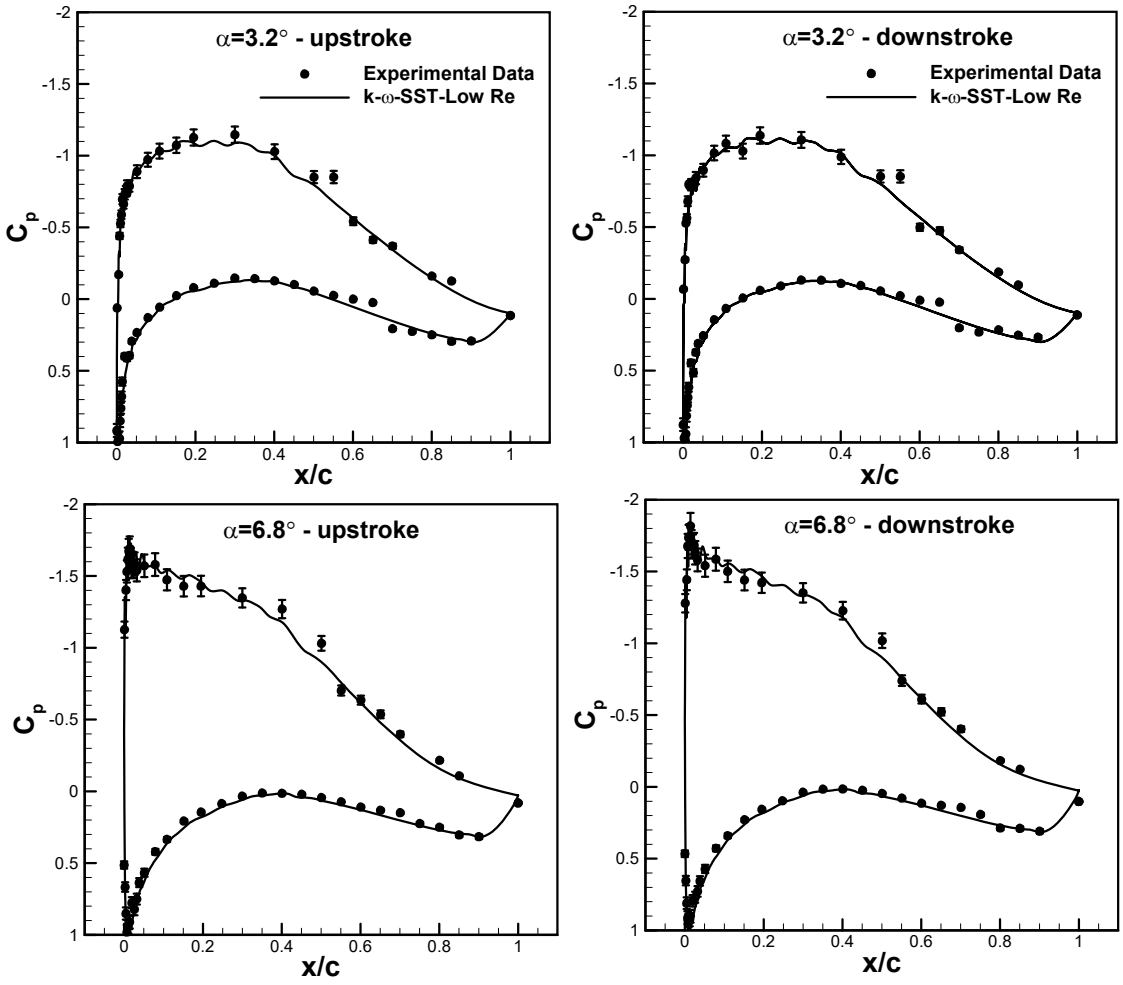

Fig. 8 Comparison of numerical pressure coefficients and experimental data- 1st test case- α_0=5°, d=2°, k=0.025

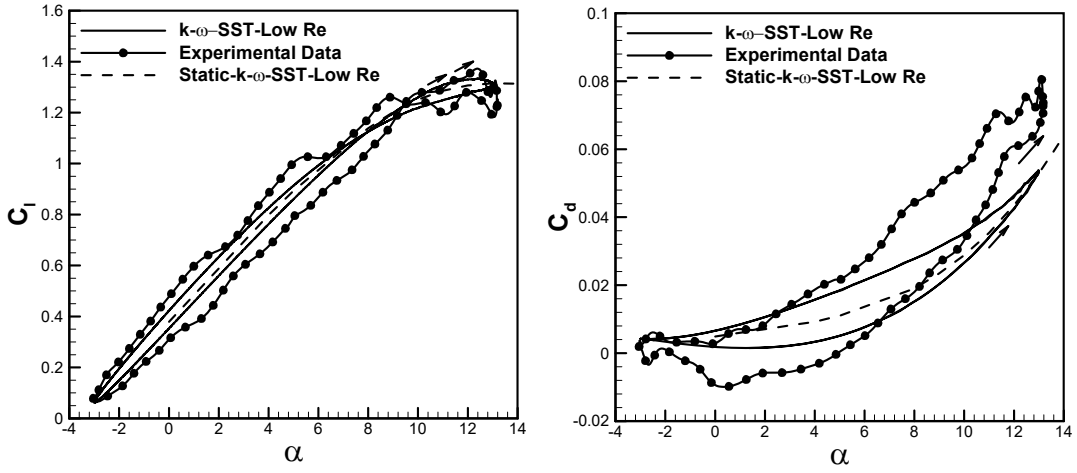

(a) (b)

Fig. 9 Aerodynamic coefficients- 2nd test case- α_0=5°, d=8°, k=0.025

C. Pitching Airfoil; Near-Static Stall Case

The airfoil in this case executes the harmonically oscillating motion under the equation $\alpha = 5 + 8\sin(\omega t)$. Exceeding the static stall angle, the viscous effects impact the flow structures. However, the maximum AoA in this case is 13° and consequently, only limited vortex formation occurs in this region and there is no severe separation. As a result, the dynamic stall happens in the form of the growth in the lift

coefficients at AoAs beyond the static stall. Fig. 9 indicates the lift and drag coefficients loops for our numerical simulation and the experimental data. The lift coefficient loop suggests that, at the end of the upstroke motion, a slight drop-off occurs which is due to the formation and movement of the dynamic stall vortex on the upper surface of the airfoil. To confirm this statement, the streamlines are presented in Fig. 10. As seen, in the upstroke motion at α=8°, a vortex is forming at the trailing edge region of the upper surface. The vortex is expanding by increasing the AoA. At the end of the upstroke motion, very small movement of the vortex happens which leads to small drop in the lift coefficient. As the airfoil starts the downstroke motion, the lift coefficient decreases as well. The phase-lead of the lift coefficients turns into the lag one at α=8°.

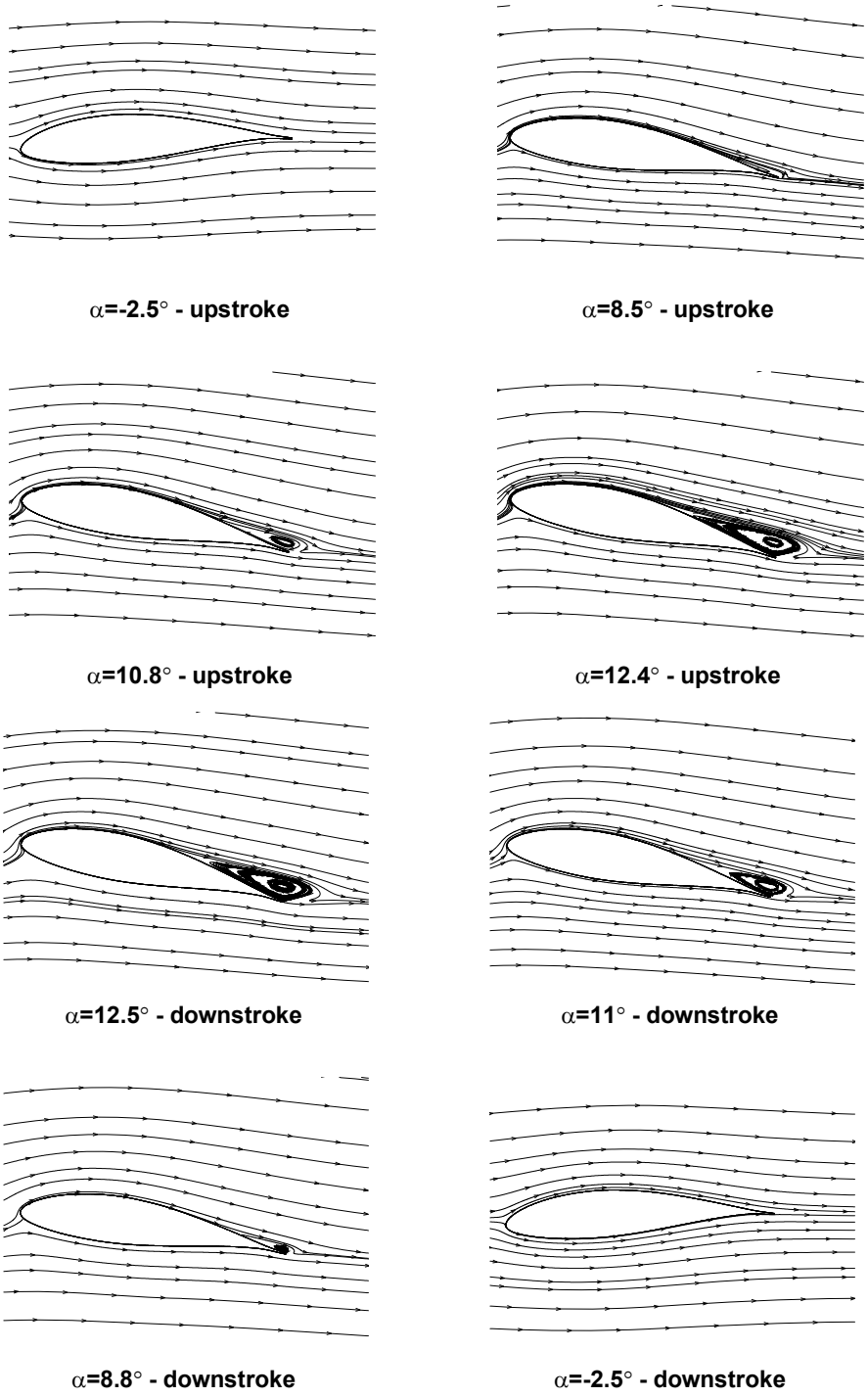

Fig. 10 Streamlines- 2nd test case- α_0=5°, d=8°, k=0.025

Fig. 11 shows the pressure distributions around the airfoil at different AoAs. Same as the previous case, the pressure coefficient values are properly predicted on the lower surface of the airfoil. As seen in Fig. 11, at α=12.5° for both the upstroke and downstroke motions, the length of the flat area in pressure coefficient curve is slightly different for the numerical and experimental curves. This area corresponds to the size of the vortex formed on the upper surface of the airfoil. The URANS method predicts larger vortex at the trailing edge region causing the discrepancy.

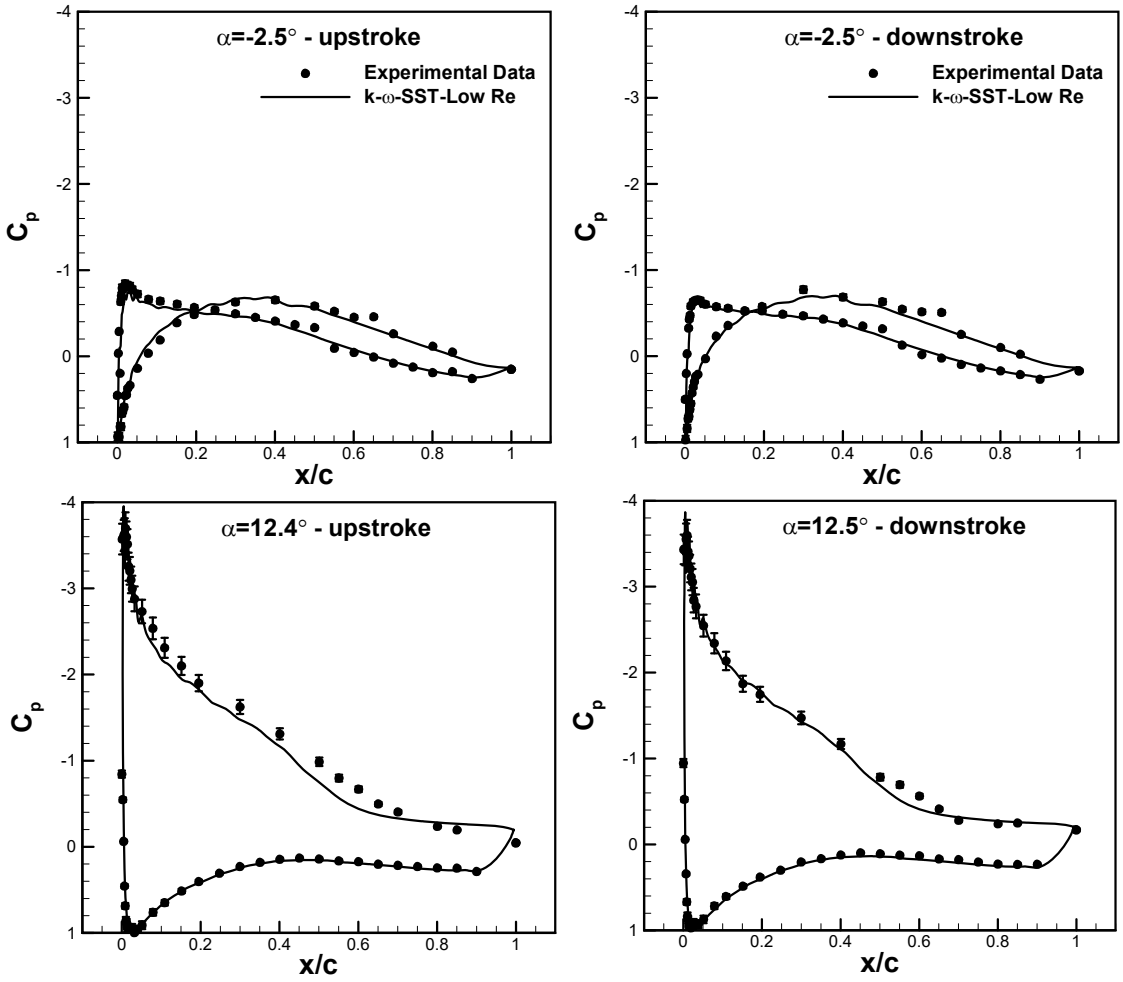

Fig. 11 Comparison of numerical pressure coefficients and experimental data- 2ndt test case- α_0=5°, d=8°, k=0.025

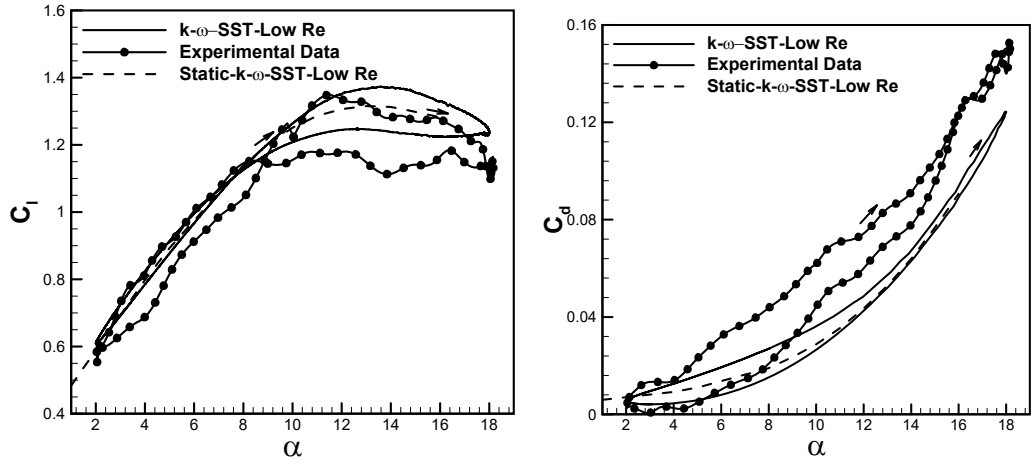

(a) (b)

Fig. 12 Aerodynamic coefficients- 3rd test case- α_0=10°, d=8°, k=0.025

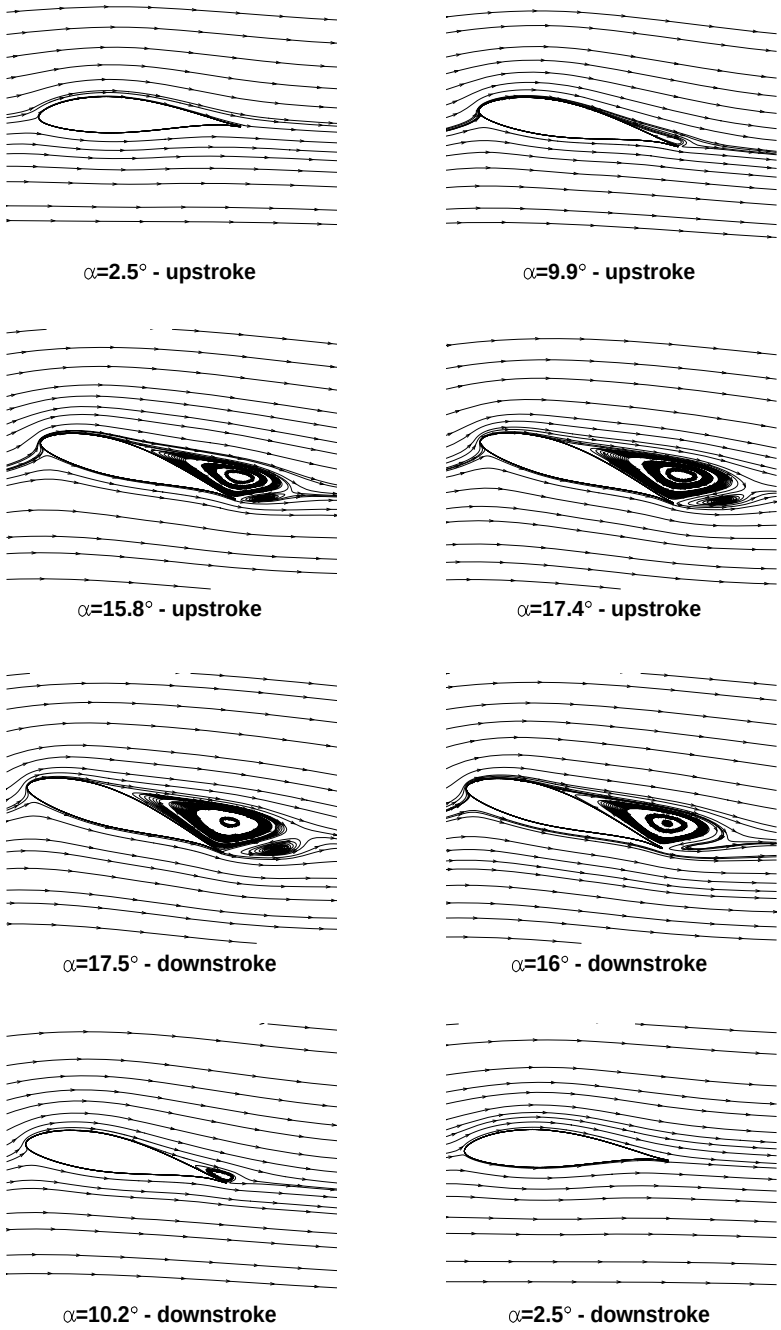

Fig. 13 Streamlines- 3rd test case- α_0=10°, d=8°, k=0.025

D.Pitching Airfoil; Post-Static Stall Case

In this case, the airfoil motion far exceeds the static stall AoA. The mean AoA is 10° and the airfoil oscillates with the amplitude of 8°. Fig. 12 represents the hysteresis loops of the lift and pressure drag coefficients for the numerical simulation and the experimental data. The crossover of the lift coefficient curves in the upstroke and downstroke motions occurs at α=8.5°. The predicted intersection point by our numerical simulations has a good agreement with the corresponding point in the experiment. The intersection point is the turning point of the lift curves in the upstroke and downstroke motions where the phase-lead turns into the phase lag during the downstroke motion.

The flow pattern of this case (Fig. 13) expresses a vortex formed on the upper surface which is expanding at a constant region until α=13°. Afterward, the vortex starts to move toward the trailing edge. According to Fig. 13, the dynamic stall regime is characterized by the formation of the trailing edge vortex, and the traveling of this vortex towards downstream causes the drop-off the lift coefficient.

The vortex formation for most of the airfoils like NACA0012 occurs at leading-edge. However, the vortex formation locates at the trailing edge for the studied airfoil. The formation of trailing-edge vortex for this airfoil is attributed to the geometry of the airfoil including the curvature and thickness of the airfoil.

Based on the pressure distributions around the airfoil depicted in Fig. 14, the flow velocity on the upper surface increases by growing the AoA, and consequently, the value of the suction peak rises. It is qualitatively noticeable that the changes in the suction peak value and separation area cause the difference between the lift coefficients at $\alpha \geq 10°$ in the upstroke and downstroke motions. At high AoAs, the dynamic stall vortex formed at the trailing edge of the airfoil is the reason of the increase in the pressure coefficient curve at the trailing-edge region. In addition to the sources of discrepancies mentioned in previous sections, there have been some restrictions in experiments to install the pressure sensors at the trailing-edge and the leading edge of the studied airfoil. Therefore, the number of the sensors on these regions was limited, and their locations had some limitations. As a result, the pressure distributions were not obtained completely. This can express part of the discrepancy observed on the pressure distribution at the trailing edge region.

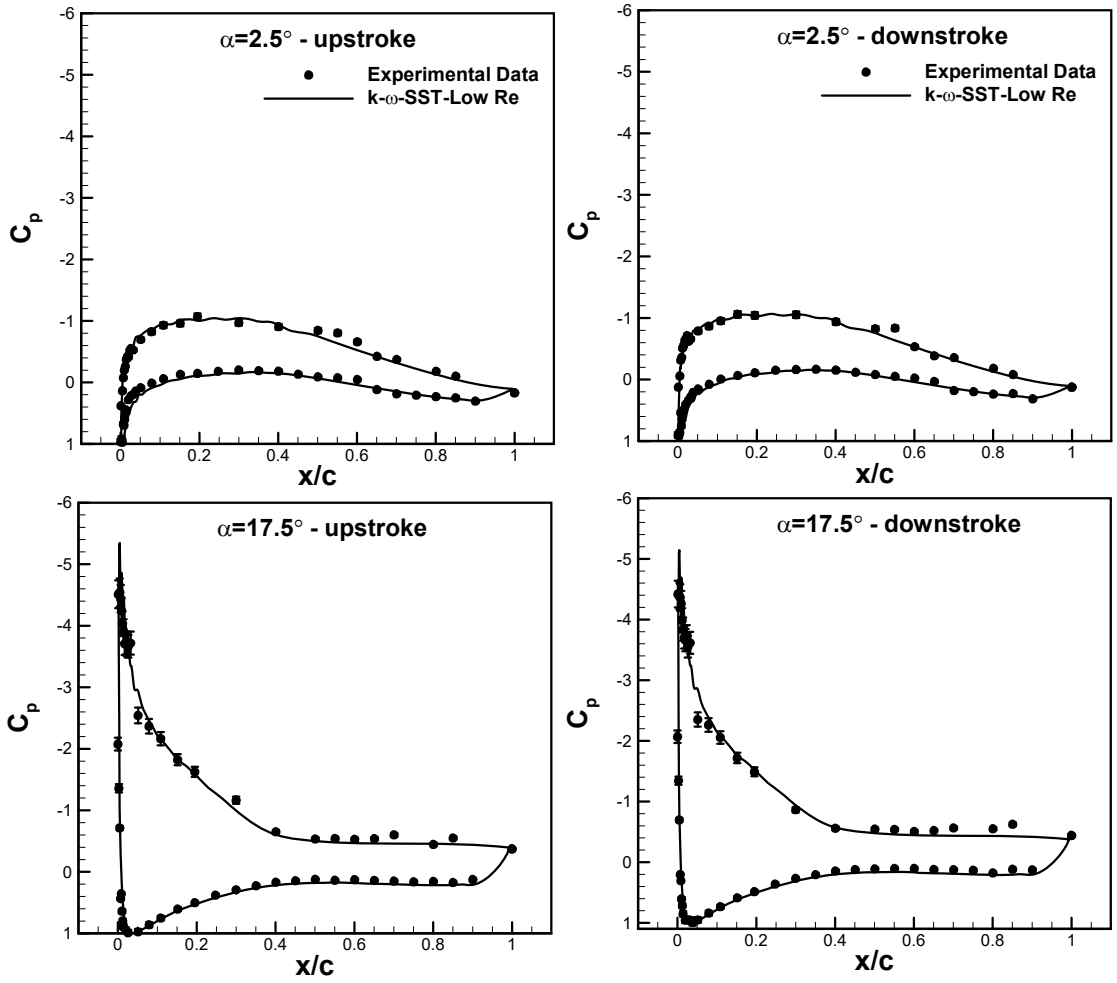

Fig. 14 Comparison of numerical pressure coefficients and experimental data- 3rd test case- α_0=10°, d=8°, k=0.025

IV. Conclusion

In this study, the aerodynamic behavior of a stationary and oscillating NACA 6-series airfoil was investigated. Using URANS equations along with a proper turbulence model ($k-\omega-SST$ with low-Re correction), the aerodynamic and pressure coefficients of the oscillating airfoil at pre-, near- and post-static stall regions were calculated and the flow patterns were simulated as well. Due to the vortex formation and uncertainty in turbulent flows, the CFD results illustrate that it is an ongoing challenge to predict the aerodynamic coefficients accurately by URANS models. However, having chosen appropriate turbulence model ($k-\omega-SST$ with low-Re correction) and setting the turbulence values correctly besides the mesh refinement, it was shown that the reliable results which were obtained can be validated with the corresponding experimental data.

For stationary airfoil, the angle of static stall for numerical simulation is posterior to the corresponding experimental data. Also, the amount of lift coefficients is higher than experimental results. At very low AoAs, the drag coefficients

have high accuracy, while the accuracy decreases by increasing the AoA. Two-dimensional turbulence modelling and considering the whole domain as turbulent flow lead to posterior prediction of the vortex on the upper surface and the separation phenomenon as well. These parameters along with experimental errors and wall effects cause the discrepancies observed in aerodynamic coefficients. Furthermore, it is worth mentioning that the pressure coefficients are measured by pressure sensors in experimental tests. As a result, due to the restrictions of installing the sensors on the leading- and trailing edges, the correct measurement of pressure at these locations are impossible. Therefore, the measurement of pressure distribution of total points around the airfoil has not been made. Consequently, the aerodynamic coefficients would have some error as well due to the integration of the pressure coefficient diagrams. Utilizing force balance could lead to more accurate results in experimental data.

For oscillating airfoil, at pre-stall region, the viscous effects are negligible, and therefore, no zero-pressure gradient and separation occur at the upper surface of the airfoil. However, at near- and post-stall regions, the flow over the upper surface separates and due to the high curvature and 15% thickness of the airfoil, a vortex forms at the trailing-edge region. In the studied cases, the hysteresis loops of the lift and pressure drag coefficients and also, the pressure distribution around the airfoil for numerical results are similar to the corresponding experimental data. Using $k-\omega-SST$ with low-Re correction with grid satisfying y^+ less than 1 in OpenFOAM, we showed that in spite of the existence of adverse pressure gradients, flow separation and vortex formation at near- and post-stall regions (especially in upstrokes), high accurate predictions of the aerodynamic and pressure coefficients can be achieved.

REFERENCES

[1] D. Shipley, M. Miller, M. Robinson, "Dynamic Stall Occurrence on a Horizontal Axis Wind Turbine Blade," Technical Report, NREL/TP-442-6912, National Renewable Energy Laboratory, 1995.

[2] C. P. Butterfield, "Aerodynamic pressure and flow visualisation measurement from a rotating wind turbine blade," in *Proc. 8th ASME Wind Energy Sumposium,* Houston, Texas, 1989.

[3] K. W. McAlister, L. W. Carr, W. J. McCroskey, "Dynamic stall experiments on the NACA0012 airfoils," Technical Report, NASA, paper 1100, 1978.

[4] W. J. McCroskey, L. W. Carr, K. W. McAlister, S. L. Pucci, "An experiment study of dynamic stall on advanced airfoil sections," Technical Report, NASA TM-84245, 1982.

[5] W. J. McCroskey, "The Phenomenon of Dynamic Stall," Technical Report, NASA TM-81264, 1981.

[6] W. J. McCroskey, "Unsteady Airfoils", *Annual Review of Fluid Mechanics,* vol. 14, pp. 285-311, 1981.

[7] L. W. Carr, "Progress in Analysis and Prediction of Dynamic Stall," *Journal of Aircraft,* vol. 25, No. 9, pp. 6-17, 1988.

[8] R.A. Piziali, "2-D and 3-D oscillating wing aerodynamics for a range of angles of attack including stall." Technical Report TR 94-A001. NASA; 1994.

[9] J. A. Ekaterinaris, F. R. Menter. "Computation of oscillating airfoil flows with one-and two-equation turbulence models." *AIAA J.* vol. 32(12), pp.2359–65, 1994.

[10] G. N. Barakos, D. Drikakis, "Unsteady separated flows over manoeuvering lifting surfaces," *Philosophical Transactions of The Royal Society,* vol. 358, pp. 3279-3291, 2000.

[11] T. N. Nandi, J. Brasseur, and G. Vijayakumar, "Prediction and Analysis of the Nonsteady Transitional Boundary Layer Dynamics for flow over an Oscillating Wind Turbine Airfoil using the γ-Reθ ransition Model," 34th Wind Energy Symposium. San Diego, California, USA.

[12] M. R. Amiralaei, H. Alighanbari, S. M. Hashemi, "An investigation into the effects of unsteady parameters on the aerodynamics of a low Reynolds number pitching airfoil," *Journal of Fluids and Structures,* vol. 26, pp. 979-993, 2010.

[13] K. Lu, Y.H. Xie, D. Zhang, "Numerical study of large amplitude, nonsinusoidal motion and camber effects on pitching airfoil propulsion." *Journal of Fluids and Structures*, vol. 36, pp. 184–194, 2013a.

[14] D. Poirel, V. Me´tivier, G. Dumas, "Computational aeroelastic simulations of self-sustained pitch oscillations of a NACA0012 at transitional Reynolds numbers." *Journal of Fluids and Structures*, vol. 27, pp. 1262–1277, 2011.

[15] T. Lee, P. Gerontakos. "Investigation of flow over an oscillating airfoil." *Journal of Fluid Mechanics*, vol. 512, pp. 313–341, 2004.

[16] G. Martinat, M. Braza, Y. Hoarau, G. Harran, "Turbulence modelling of the flow past a pitching NACA0012 airfoil at 10^5 and 10^6 Reynolds numbers," *J. Fluids Struct*. vol. 24, pp. 1294–1303, 2008.

[17] S. Wang, D.B. Ingham, L. Ma, M. Pourkashanian, Z. Tao. "Numerical investigations on dynamic stall of low Reynolds number flow around oscillating airfoils." *Comput Fluids vol.* 39, pp. 1529–41, 2010.

[18] S. Wang, D.B. Ingham, L. Ma, M. Pourkashanian, Z. Tao. "Turbulence modeling of deep dynamic stall at relatively low Reynolds number." *J Fluids Struct*, vol. 33, pp. 191–209, 2012.

[19] K. Lu, Y. H. Xie, D. Zhang, J. B. Lan. "Numerical investigations into the asymmetric effects on the aerodynamic response of a pitching airfoil." *Journal of Fluids and Structures,* vol. 39, pp. 76–86, 2013b.

[20] K. Gharali K, D. A. Johnson, "Dynamic stall simulation of a pitching airfoil under unsteady freestream velocity." *J Fluids Struct*, vol. 42, pp. 228–44, 2013.

[21] G. H. Yu, X. C. Zhu, Z. H. Du, "Numerical simulation of a wind turbine airfoil: dynamic stall and comparison with experiments", *Journal of Power and Energy,* Vol. 224, No. 5, pp. 657-677, 2010.

[22] Z. Zhou, C. Li, J. B. Nie, Y. Chen, "Effect of oscillation frequency on wind turbine airfoil dynamic stall," *IOP Conf. Series: Materials Science and Engineering*, Vol. 52, 2013.

[23] S. Nagarajan, S. Hahn, S. Lele, "Prediction of sound generated by a pitching airfoil: a comparison of RANS and LES." In *Proc AIAA/CEAS aeroacoustics conference,* Cambridge, Massachusetts, 2006.

[24] Y. Kim, Z. T. Xie, "Modelling the effect of freestream turbulence on dynamic stall of wind turbine blades," *Computers and Fluids,* Vol. 129, pp. 53-66, 2016.

[25] OpenFOAM. *User guide 2.3.1*. Technical Report. OpenFOAM ®, 2014; http://www.openfoam.com/documentation/user-guide/.

[26] E. Dumlupinar, V. R. Murthy, "Investigation of dynamic stall of airfoils and wings by CFD," *29th AIAA Applied Aerodynamics Conference,* Honolulu, Hawaii, 2011.

[27] A. F. M. Correa, T. P. Sales, D. A. Rade, F. J. Souza, "Study of the flow over an oscillating NACA0012 airfoil," *National congress of mechanical engineering (CONEM 2014)*, Uberlandia, Brazil, Aug 10–15, 2014.

[28] P. R. Spalart, S. R. Allmaras, "A One-Equation Turbulence Model for Aerodynamic Flows," *Recherche Aerospatiale*, No. 1, pp. 5-21, 1994.

[29] F. R. Menter, "Two-equation eddy-viscosity turbulence models for engineering applications," *AIAA Journal,* Vol. 32, No. 8, pp. 1598-1605, 1994.

[30] H.R. Karbasian, J.A. Esfahani, E. Barati, "Effect of acceleration on dynamic stall of airfoil in unsteady operating conditions." *Wind Energy* 2014.

[31] H. Jasak, Z. Tukovic, "Automatic Mesh Motion for the Unstructured Finite Volume Method," *Transactions of FAMENA*, Vol. 30, pp. 1-20, 2006.

[32] M. Lin, H. Sarlak, "A comparative study on the flow over an airfoil using transitional turbulence models," *AIP Conference Proceedings* 1738 (1), 030050, 2016.